High efficiency of Brillouin scattering behavior in single-mode Ge–As–Se–Te fibers at 2 μm

Yue Fu(付悦)[1,2,3], Shi-Xun Dai(戴世勋)[1,2,3,†], Lu-Lu Xu(徐路路)[1,2,3], Yao-Jun Fang(方耀俊)[4], Ying-Ying Wang(王莹莹)[1,2,3], Kai Jiao(焦凯)[1,2,3], and Xun-Si Wang(王训四)[1,2,3]

[1] *Laboratory of Infrared Materials and Devices, The Research Institute of Advanced Technologies, Ningbo University, Ningbo* 315211, *China*
[2] *Key Laboratory of Photoelectric Materials and Devices of Zhejiang Province, Ningbo* 315211, *China*
[3] *Engineering Research Center for Advanced Infrared Photoelectric Materials and Devices of Zhejiang Province, Ningbo* 315211, *China*
[4] *Faculty of Electrical Engineering and Computer Science, Ningbo University, Ningbo* 315211, *China*

(Received 21 June 2022; revised manuscript received 8 October 2022; accepted manuscript online 14 October 2022)

The Brillouin characteristics of step-index Ge–As–Se–Te (GAST) fibers at 2 μm are designed and simulated on the basis of optical and acoustic properties. The refractive indexes of $Ge_{20}As_{20}Se_{45}Te_{15}$ glass and $Ge_{20}As_{20}Se_{43}Te_{17}$ glass serving as fiber core and cladding are 3.20 and 3.18 at 2 μm, and their acoustic velocities are 2200 m/s and 2300 m/s, respectively. Numerical results indicate that the stimulated Brillouin scattering (SBS) efficiency is 248 $m^{-1}\cdot W^{-1}$, and the Brillouin threshold power is 66 mW when the core diameter of the 2-m-long GAST fiber is 4 μm at 2-μm wavelength. The optic–acoustic coupling factor, the Brillouin frequency shift, and the Brillouin gain coefficient are 0.98, 7.02 GHz, and 3.81×10^{-9} m/W, respectively. The SBS effect of GAST fibers simulated for the first time provides a new promising approach to selecting gain medium based on 2-μm-wavelength fiber laser.

Keywords: stimulated Brillouin scattering, chalcogenide fiber, nonlinear effect, optical–acoustic coupling

PACS: 42.55.Wd, 42.65.Es, 42.81.–i, 78.20.Pa **DOI:** 10.1088/1674-1056/ac9a3a

1. Introduction

Stimulated Brillouin scattering (SBS) is a nonlinear interaction between pump wave and Stokes wave through acoustic waves in optical fibers, which has been utilized extensively in Brillouin lasers, fiber amplifiers, optical filters, and fiber sensing due to its advantages of low threshold power, narrow gain linewidth, and high conversion efficiency.[1–4] Brillouin laser based on the SBS effect is a potential technique for obtaining lasers with extremely narrow linewidth and low noise.[5] Owing to the absorption peak of water molecules located at 2 μm, the 2-μm laser has significant application value in biomedicine, industrial processing, and other fields, which enables the rapid absorption of powerful laser energy by water.[6] The Brillouin fiber laser at 2 μm has been extensively studied. Wang *et al*. constructed a multi-wavelength Brillouin fiber laser at 1.97 μm, where the Brillouin gain coefficient (g_B) of the SMF-28 fiber is 2.89×10^{-11} m/W, and five Stokes lines with a channel spacing of roughly 0.105 nm have been obtained.[7] Luo *et al*. constructed a single-frequency 2-μm Brillouin fiber laser by using a two-stage thulium-doped fiber amplifier, with an output power of 1.08 W and a transmission efficiency of 51%.[6] However, the gain medium of the Brillouin fiber laser at 2 μm is mostly conventional silicon fiber, which has a low g_B and a high pump threshold power (the pump threshold power reached 1.08 W[6]). Shorter optical fiber leads to higher pump power, whereas longer optical fiber increases system energy consumption and is detrimental to device miniaturization. Searching for new Brillouin working medium and exploring non-waveguide Brillouin laser can alleviate the current bottleneck of Brillouin lasers. Thus, exploring Brillouin working medium with short fiber length, low Brillouin threshold power, and high g_B is necessary.

The g_B is closely related to the effective refractive index (n_{eff}) of the material, due to the fact that based on its formula, it is proportional to the eighth power of the n_{eff} of the glass.[8] The chalcogenide glass (ChG) has high nonlinear coefficient (γ, 2–3 orders of magnitude of silica) and ultra-wide infrared transmittance characteristics, presenting unique advantages in low threshold Brillouin fiber laser. Abedin *et al*. have measured a g_B of 6×10^9 m/W and an effective mode area (A_{eff}) of 39 μm^2, and revealed an effective gain efficiency (g_B/A_{eff}) at 1.55 μm that is 513 times greater than the counterpart in standard silica fibers for a 5-m-long As_2Se_3 single-mode fiber.[9] This suitable parameter (g_B/A_{eff}) can be used to directly characterize SBS efficiency and Brillouin threshold power in small core fiber.[10] Florea *et al*. reported that the threshold power is 27 mW at 1.56 μm for a 10-m-long As_2S_3 fiber.[11] Tow *et al*. constructed a Brillouin fiber ring laser by using a 3-m-long $Ge_{10}As_{22}Se_{68}$ chalcogenide photonic crystal fiber (PCF) with a Brillouin frequency shift (BFS) of 7.25 GHz and a gain linewidth of 17 MHz (the g_B is 3.3×10^{-9} m/W).[12] Wang *et al*. proposed a Brillouin fiber laser with a Brillouin laser threshold of 14 mW (the g_B is 3.9×10^{-9} m/W) on the basis of a 4.2-m-long As_2S_3 step-index fiber.[13] It is undeniable that

†Corresponding author. E-mail: daishixun@nbu.edu.cn

© 2023 Chinese Physical Society and IOP Publishing Ltd

high g_B and low Brillouin threshold power are beneficial to obtaining efficient Brillouin effect. Contrastingly, few researches have been reported in the 2-μm waveband. Hu *et al*. demonstrated a Brillouin laser on the basis of an $As_{38}Se_{62}$ suspended-core fiber with a threshold power of 91.4 mW at 2 μm (the g_B is 3.5×10^{-9} m/W).[14] Deroh *et al*. compared and analyzed the SBS characteristics of different infrared glass-based optical fibers at 2 μm.[10] Overall, the high γ of ChG is conducive to the SBS effect. However, the high-efficiency Brillouin properties of chalcogenide fibers other than As–S and As–Se-based fibers have not been reported in the 2-μm waveband because the tuning of core size, numerical aperture (NA), and the third-order nonlinear coefficient are limited by glass materials.

In this work, a novel SBS component (Ge–As–Se–Te) fiber is designed and simulated to obtain efficient SBS, thereby achieving high gain efficiency of short fiber. We investigate the effects of GAST fibers with different core diameters on the optic–acoustic coupling efficiency, g_B and Brillouin threshold power, as well as the BFS and BGS of various higher-order acoustic modes. Conclusively, the numerical results of GAST fibers can provide scientific reference for chalcogenide fibers with high Brillouin effect at 2 μm based on GAST glass with extremely wide transmission range and high nonlinear characteristics.

2. Experiments

Ge element addition improves nonlinear characteristics and trace Te element can not only increase the nonlinear refractive index (n_2) of ChG to become the largest in all glasses based on commercially available As_2S_3 and As_2Se_3 fibers, but also minimally influence fiber loss after forming.[15,16] The n_2 of Ge–Se–Te fiber increased up to 3.71×10^{-17} m^2/W and the γ reached ~ 8.727 $m^{-1}\cdot W^{-1}$.[16] Therefore, the Brillouin characteristics of the step-index $Ge_{20}As_{20}Se_{45}Te_{15}$ (GAST) fiber at 2 μm were designed and simulated through the finite element method (FEM) on the basis of the optical properties of the fiber core and cladding glass provided in this work. Therefore, Ge–As–Se–Te glasses were prepared through distillation with Mg Getter to remove oxidized impurities and purify glasses. Then, a novel isolated extrusion technology was used to extrude the $Ge_{20}As_{20}Se_{45}Te_{15}$ core rod and $Ge_{20}As_{20}Se_{47}Te_{13}$ cladding rod into the prefabricated rod.[17] The thermal stability of $Ge_{20}As_{20}Se_{15}Te_{45}$ reached 140 °C, indicating its excellent fiber forming performance after differential scanning calorimetry (DSC) analysis. The Perkin-Elmer Lambda 950 UV-VIS-NIR spectrophotometer was used to record the visible transmission spectra of the samples ranging from 400 nm to 2800 nm, and the IR transmission spectra of samples in a range of 4000 cm^{-1}–400 cm^{-1} were obtained by a Nicolet 380 Fourier infrared spectrophotometer. The refractive index of the core and cladding glass were measured by an IR ellipsometer (IR-VASE MARK II, J. A. Woollam Co.).

3. Modeling theory

The SBS process refers to the annihilation of an incident field photon (pump light), producing a Stokes photon with downshifting frequency and an acoustic phonon that preserves momentum and energy conservation. Pump waves generate acoustic waves through electrostriction, which in turn modulate the refractive index of the medium.[18] In this paper, the FEM was first used to solve the optical-wave equation and the acoustic equation to obtain the optical mode field $\boldsymbol{E}$ and the acoustic mode field $\boldsymbol{u}$.[19] The equation is expressed as a two-dimensional (2D) vector wave equation as follows:[20]

$$\nabla_t^2 \boldsymbol{E} + \left(\frac{2\pi}{\lambda}\right)(n^2 - n_{\text{eff}})\boldsymbol{E} = 0, \tag{1}$$

$$\nabla_t^2 \boldsymbol{u} + \left(\frac{\omega_a^2}{v^2} - \beta_a^2\right)\boldsymbol{u} = 0, \tag{2}$$

where ∇_t^2 is the transverse Laplace operator, λ is the pump wavelength, n_{eff} is the effective refractive index, v is the velocity of the acoustic mode, and ω_a is the angular frequency of the acoustic wave.[21] In the GAST fiber model established in this work, λ is 2 μm, the value of v is 2200 m/s for core glass and 2300 m/s for cladding glass. Back SBS occurs only when the acoustic propagation constant $\beta_a = 2\beta_{\text{opt}}$ meets the phase matching condition, where $\beta_{\text{opt}} = 2\pi n_{\text{eff}}/\lambda$ is the optical propagation constant.

The coupling degree of the fundamental mode of the optical field and the i-th order acoustic field is expressed by the coupling integral I_i, and it is given by[21]

$$I_i = \frac{\left(\iint |\boldsymbol{E}(x,y)|^2 \boldsymbol{u}_i^*(x,y)\,\mathrm{d}x\mathrm{d}y\right)^2}{\iint |\boldsymbol{E}(x,y)|^4\,\mathrm{d}x\mathrm{d}y \iint |\boldsymbol{u}_i(x,y)|^2\,\mathrm{d}x\mathrm{d}y}, \tag{3}$$

where $\boldsymbol{E}(x,y)$ represents the mode intensity of the fundamental mode of the optical field, and $\boldsymbol{u}_i(x,y)$ denotes the mode intensity of the fundamental mode or higher-order mode of the acoustic field.[22]

The BFS of the i-th order acoustic mode is expressed as[23]

$$f_{B,i} = \frac{\omega_{a,i}}{2\pi}. \tag{4}$$

The Brillouin gain spectrum (BGS) corresponding to the i-th order acoustic mode exhibits a Lorentz curve distribution[23] and it is given by

$$S_{B,i}(f) = g_0 \frac{(\Delta f_B/2)^2}{(f - f_{B,i})^2 + (\Delta f_B/2)^2}, \tag{5}$$

where g_0 is the peak value of Brillouin gain at $f = f_{B,i}$, and $g_0 = g_{B,i}I_i$. Δf_B is the full linewidth at half-maximum

(FWHM) of the BGS, and the estimated value of the GAST fiber here is 25 MHz. $g_{B,i}$ is given by

$$g_{B,i} = \frac{4\pi n_{\text{eff}}^8 p_{12}^2}{\lambda^3 \rho c f_{B,i} \Delta f_{B,i}}, \tag{6}$$

where $\rho = 5208$ kg/m^3 and $p_{12} = 0.251$ are the density of the GAST core glass and the longitudinal photo-elastic coefficient, respectively; $\rho = 5157$ kg/m^3 is the density of the GAST cladding glass; c is the speed of light in a vacuum. Given that all acoustic modes are statistically independent, the total BGS of the GAST fiber is the sum of each mode.[21]

The pump power becomes the Brillouin threshold power when it reaches a critical value, which is related to g_B by[24]

$$P_{\text{th}} = \frac{21KA_{\text{eff}}}{g_B L_{\text{eff}}}, \tag{7}$$

where A_{eff} is the optical effective mode area, K is the polarization factor, L_{eff} is the effective length, which is defined as $L_{\text{eff}} = 1 - \exp(-\alpha l)/\alpha$, and α is the loss factor of the fiber.[24,25]

4. Simulation results and discussion

4.1. Optical parameters of glass

The NIR and IR transmission spectra of the $Ge_{20}As_{20}Se_{45}Te_{15}$ glass and $Ge_{20}As_{20}Se_{47}Te_{13}$ glass are shown in Fig. 1. Figure 1(a) exhibits no obvious absorption peak of oxidized impurities in the transmission spectra of the glasses, and the transparency extends from 1.5 μm to 18 μm. The transmittance of the core and cladding reach 56.6% and 53.1% at 2 μm as shown in Fig. 1(a). Moreover, figure 1(b) shows that the GAST glass maintains a relatively high transmittance ina longwave infrared range, which provides a reference for the future study of the Brillouin effect of long-wave fibers.

The measured linear refractive indices of the fiber are shown in Fig. 2(a), demonstrating that the refractive indexes of the core and cladding are 3.20 and 3.18 at 2 μm, respectively. The step-index GAST fiber is beneficial to obtaining SBS with higher gain peak value because the high refractive index of the fiber core indicates that it has high nonlinear characteristics when the wavelength is less than 2.5 μm. Figure 2(a) also shows that the calculated NA of the stepindex GAST fiber is 0.37 when the working wavelength is 2 μm, suggesting an appropriate NA ensures that when light is transmitted in a single mode, the core diameter is not too small to be successfully manufactured. Figure 2(b) shows the size range of the core diameter, which is chosen according to the single-mode operation condition, $V < 2.405$, where V is the normalized angular frequency parameter[26] in a wavelength range of 1.5 μm–5 μm. The red dotted line indicates that the wavelength is 2 μm, which represents the core diameter range that ensures single-mode transmission of the GAST fiber at this wavelength. The maximum core diameter of single-mode transmission grows with the increase of wavelength, indicating that the core can be enlarged accordingly. In summary, the single-mode step-index GAST fiber model with a core diameter of 3 μm–4 μm at 2-μm wavelength is established in the following part.

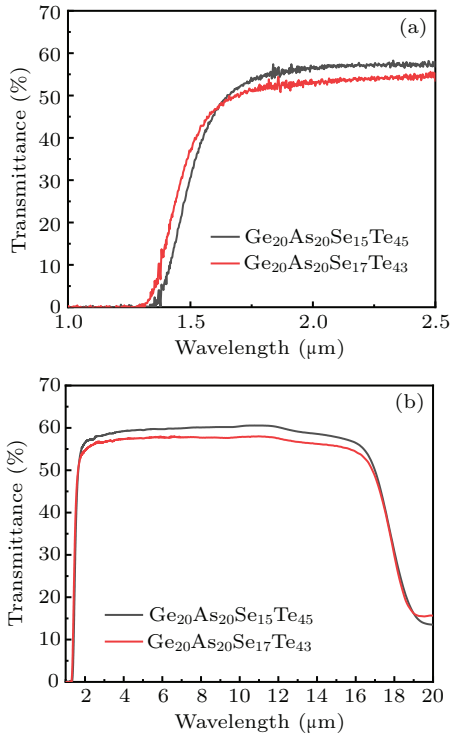


Fig. 1. Optical transmission of ∼ 2-mm-thick bulk GAST glass in (a) NIR and (b) IR.

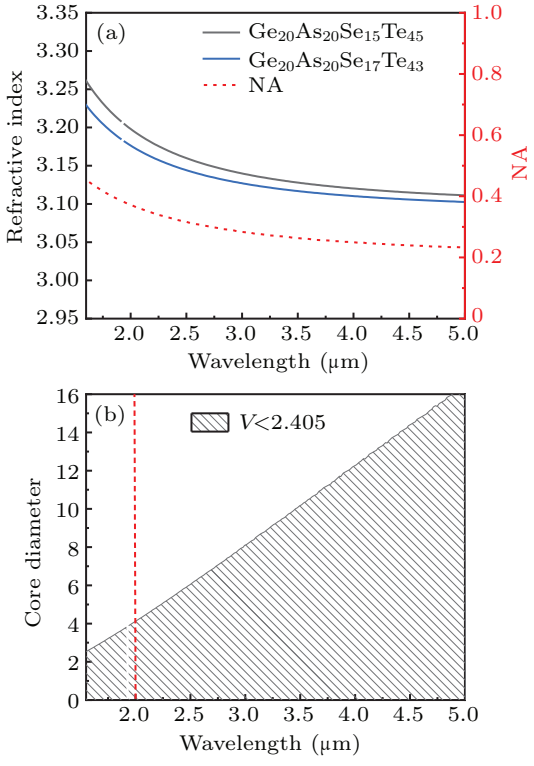


Fig. 2. (a) Curve of refractive index *versus* wavelength of GAST glass and e calculated NA, and (b) variation of core diameter range with wavelength during single-mode transmission.

4.2. Coupling efficiency of optical field and acoustic field

In this work, the FEM is used to investigate the optic–acoustic coupling effects of the designed step-index GAST fibers with different core diameters (3 μm, 3.5 μm, and 4 μm), the BGS and the variation of Brillouin threshold power with fiber length are obtained. On the basis of the all-vector solver, the fiber cross-sectional surface is divided into over 2860 non-uniform meshes, each with a minimum cell size of 0.015 μm and average cell mass of 0.88 by using the idea conductor boundary conditions, and the n_{eff} of the fundamental optical mode of the fiber is first calculated.

The fundamental optical mode (HE_{11}) distributions of the GAST fibers with different core diameters at 2 μm are obtained as shown in Fig. 3. The figure exhibits that when the diameter of the fiber core is small, there will transpire a small amount of optical field leakage, whereas as the diameter of the fiber core increases, the electric field energy gradually increases and concentrates in the fiber core. The ratio of the fiber diameter to the optical field leakage diameter is the smallest when the fiber diameter is 3 μm, so the degree of optical field leakage is the strongest in Fig. 3. Therefore, increasing the core diameter appropriately is more advantageous for the optical field's energy concentration. Then, the n_{eff} can be used to obtain the distribution of acoustic field mode satisfying the relation between β_{a} and β_{opt}.

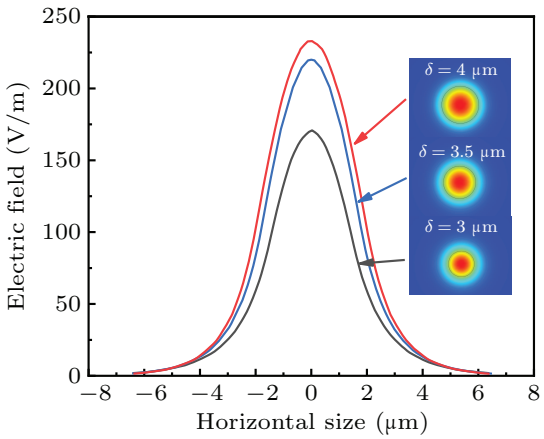


Fig. 3. Fundamental optical mode (HE_{11}) distributions of GAST fiber with different core diameters.

The fundamental and higher-order acoustic modes of the GAST fiber at 2 μm are calculated when the core diameter is 3 μm and 4 μm, as shown in Fig. 4. As can be seen from the figure, the distributions of fundamental acoustic mode (R_{01}) and higher-order acoustic modes (R_{02} and R_{03}) in the step-index GAST fiber are all axisymmetrical in the cross section of the fiber and confined in the fiber core.[27] Thus, the energy is not easy to leak into the cladding when the core diameter of the same acoustic mode is larger within the adjustable range. The energy distributions and strengths of various acoustic modes in the fiber core are different. Among them, the energy of R_{01} from the core to the cladding is decreasing and the ultimate value is higher than that of R_{02}, while the energy distribution along the radial direction of the core in the higher-order acoustic mode is not monotonically decreasing.

The variation of the acoustic pressure distribution along the diameter of the fiber section is shown in Fig. 5. Figure 5(a) shows the acoustic field distribution of R_{01}, R_{02}, and R_{03} when the core diameter is 3 μm. In Fig. 5(b), the higher-order acoustic mode of the fiber core with a diameter of 4 μm has one more mode (R_{04}) than that of the fiber with a smaller size. These higher-order acoustic modes can be collectively referred to as shear acoustic modes (SAM), and their phase velocities are usually smaller than the bulk shear velocities of the cladding material.[27] Assuming that the frequency of its acoustic field is limited by $V_{\text{core}} < 2\pi f_m^{\text{a}}/\beta_{\text{a}} < V_{\text{clad}}$, there exists an additional higher-order mode, where β_{a} is the acoustic propagation constant, f_m^{a} is the acoustic frequency of the m-th acoustic mode, V_{core} and V_{clad} are the acoustic velocities of the fiber core and cladding when the core diameter increases.[27] The lack of R_{04} mode in 3-μm-core fiber is attributed to the influence of f_m^{a} that is limited to β_{a} value of core material and cladding material. Brillouin backscattering occurs only when the phase matching condition of the acoustic field is satisfied, and optical field is $\beta_{\text{a}} = 2\beta_0$, where $\beta_0 = 2\pi n_{\text{eff}}/\lambda$, with n_{eff} being the effective refractive index of the optical field, and λ denoting the pump wavelength. Thus, with the increase of core diameter, n_{eff} and β_{a} of the fiber core increase, and eventually the range of f_m^{a} widens, resulting in higher-order acoustic modes.

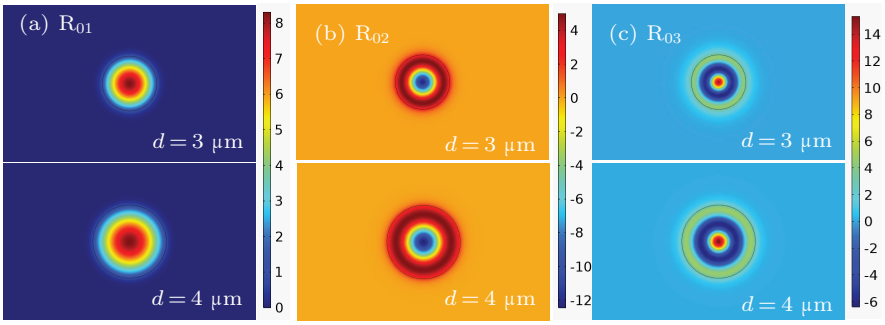


Fig. 4. Distributions of (a) R_{01} mode and higher-order modes, (b) R_{02}, and (c) R_{03} of the acoustic fields with core diameters of 3 μm and 4 μm.

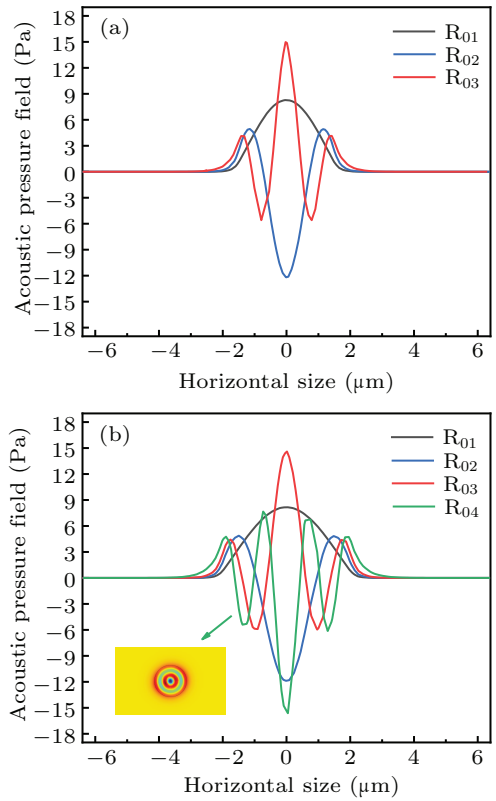


Fig. 5. Curves of horizontal-size-dependent acoustic pressure field along diameter of fiber cross-section with core diameter of (a) 3 μm and (b) 4 μm, with inset showing higher-order mode (R_{04}) distribution of acoustic field.

Moreover, as shown in Fig. 4, the maximum energy of higher-order acoustic modes concentrated in a small region in the center of the fiber core is significantly greater than that of R_{01}, indicating that the higher-order acoustic field is sensitive to the SBS effect.

To emphasize the correlation of each acoustic mode in the subsequent Brillouin gain spectrum, equation (3) is used to calculate the overlap space of optical mode and acoustic mode.[26] Figure 6 shows the optic–acoustic coupling factors corresponding to acoustic modes of different fiber diameters, and represent the coupling efficiency between the acoustic field and optical field. Two nonvanishing integral overlap values are presented, and in Fig. 6, it is confirmed that there exist more than three peaks for the GAST fiber. The coupling efficiency of the fundamental mode of the optical field and acoustic field is close to 1, whereas the coupling efficiency of the higher-order acoustic field is less than 0.1 as shown in Fig. 6. Consequently, the total strength of the fundamental acoustic field with uniform energy distribution along the core diameter is greater than that of the higher-order mode with fluctuating energy according to Fig. 5, thereby resulting in the highest optic–acoustic coupling efficiency of R_{01} in Fig. 6. Thus, the acoustic field distribution of R_{01} overlaps appropriately with the optical field. Although the peak intensity of the higher-order acoustic mode is significantly higher than that of R_{01}, the additional higher-order acoustic modes expand the fiber core to the separate part of the acoustic field energy, thus reducing its coupling efficiency.

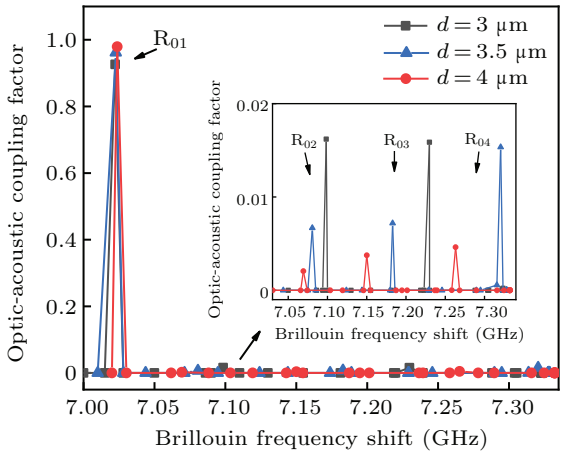


Fig. 6. Optic–acoustic coupling factors *versus* Brillouin frequency shift of the GAST fibers with different core diameters, with inset showing optic–acoustic coupling factors *versus* Brillouin frequency shift of local higher-order acoustic modes.

Table 1. BFS variation of multi-order acoustic modes.

Core diameter (μm)	BFS of R_{01} (GHz)	BFS of R_{02} (GHz)	BFS of R_{03} (GHz)	BFS of R_{04} (GHz)
3	7.022	7.098	7.230	–
3.5	7.023	7.081	7.183	7.321
4	7.024	7.069	7.150	7.265

The optic–acoustic coupling efficiency of higher-order acoustic modes decreases with the increase of the fiber core. The coupling efficiency gradually increases with the increase of the acoustic mode order, and the variation amplitude also decreases with the increase of the core when the diameter of the core is larger than 3 μm. Moreover, the BFS changes when the core diameter is different because β_{opt} and the core radius are related to the intrinsic equation of the core mode of the single-mode fiber.[27] Then, we explore the BFS variation corresponding to each higher-order mode, and the BFS parameters are listed in Table 1. As can be seen from the table, the BFS of R_{01} moves slightly toward the high frequency with the increase of the core diameter, whereas the overall BFS of the higher-order mode moves toward the low frequency, and more higher-order modes are produced due to the value of β_a increasing. At the same core diameter, the BFS diversity of various higher-order acoustic modes increases gradually; meanwhile, it decreases as the core diameter increases. In summary, the optic–acoustic coupling efficiency corresponds to a higher-order mode, and the movement of BFS is more pronounced when the core diameter is small.

4.3. Brillouin gain spectrum

The fiber structure affects the field distribution of light mode and acoustic mode, and ultimately affects the interaction between the two modes, thereby obtaining different BGS.[28] The calculated BGS of the step-index GAST fiber at 2 μm is presented in Fig. 7 to further obtain the influence of the fiber structure on Brillouin gain induced by different acoustic

modes. Referring to the influence of wavelength of chalcogenide fibers, such as the Ge–As–Se fiber and the phonon lifetime of glass, the Brillouin gain linewidth of GAST fiber is estimated at 25 MHz, which is the maximum Brillouin gain linewidth of the currently known chalcogenide fiber working at 2-μm wavelength for subsequent comparison, then, the corresponding g_B is calculated from Eq. (6).[10,12,29]

The BGS comprises three or four peaks, each corresponding to the contribution of R_{0m} acoustic mode. The GAST fiber with 3-μm-diameter core shows three peaks at the acoustic frequencies $f_{B1} = 7.02$ GHz, $f_{B2} = 7.10$ GHz, and $f_{B3} = 7.23$ GHz with the Brillouin gain coefficients $g_{B1} = 3.808 \times 10^{-9}$ m/W, $g_{B2} = 3.767 \times 10^{-9}$ m/W, and $g_{B3} = 3.7 \times 10^{-9}$ m/W, respectively, as indicated in Fig. 7. There are four peaks at the acoustic frequencies $f_{B1} = 7.02$ GHz, $f_{B2} = 7.08$ GHz, $f_{B3} = 7.18$ GHz, and $f_{B4} = 7.32$ GHz with the Brillouin gain coefficients $g_{B1} = 3.808 \times 10^{-9}$ m/W, $g_{B2} = 3.777 \times 10^{-9}$ m/W, $g_{B3} = 3.723 \times 10^{-9}$ m/W, and $g_{B4} = 3.653 \times 10^{-9}$ m/W of GAST fiber with 3.5-μm-core diameter, respectively. The peak of BGS corresponding to R_{02} is relatively low, which is weaker and invisible when the core diameter is 4 μ m. There exist four peaks at the positions of the acoustic frequencies $f_{B1} = 7.02$ GHz, $f_{B2} = 7.07$ GHz, $f_{B3} = 7.15$ GHz, and $f_{B4} = 7.27$ GHz with the Brillouin gain coefficients $g_{B1} = 3.808 \times 10^{-9}$ m/W, $g_{B2} = 3.783 \times 10^{-9}$ m/W, $g_{B3} = 3.74 \times 10^{-9}$ m/W, and $g_{B4} = 3.681 \times 10^{-9}$ m/W, respectively. The multi-peaked BGS reflects the presence of several acoustic modes at different frequencies and explains the values of the overlap integral. The overlap of optical mode and acoustic mode significantly affects the intensity of SBS. Thus, the difference in BGS is primarily attributable to the coupling coefficient of light force and the various acoustic modes.

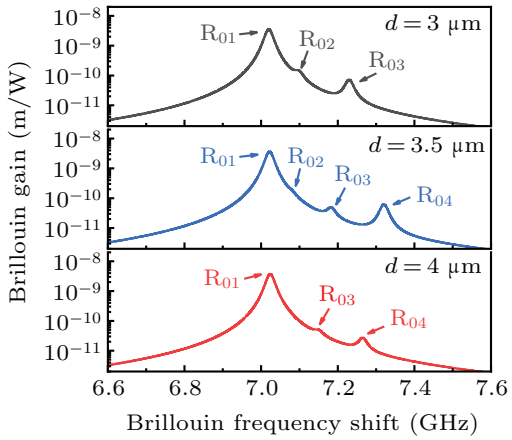


Fig. 7. Brillouin gain spectra of GAST fibers with different core diameters.

4.4. SBS threshold

Equation (7) demonstrates that the SBS threshold power decreases with the increase of fiber length on the basis of the loss of GAST fiber at 2-μm wavelength in Ref. [29] being 3 dB/m as shown in Fig. 8. The SBS threshold is 58 mW when the fiber length of 3-μm-core diameter is 2 m, which finally decreases to 37 mW as fiber length increases. The reason is that the effective length of the fiber increases to a constant with the increase of the fiber length, resulting in the gradual decrease of the SBS to a constant. Figure 8 shows that the SBS threshold of 3-μm-core diameter is lower than that of 4-μm-core diameter because the small A_{eff} and large g_B mean that the high SBS efficiency reduces the SBS threshold.

Finally, the SBS characteristics of step-index fibers with different glass substrates are compared with each other as shown in Table 2, including standard silica SMF-28, As_2S_3 fiber, As_2Se_3 fiber, and the GAST fiber. Thus, the BFSs and spectral linewidths of all the fiber samples at 2 μm are lower than those reported at 1.55-μm pump wavelength. Assuming that the Brillouin gain linewidth is inversely proportional to λ^2, it can be inferred that the Brillouin linewidth of As_2Se_3 fiber at 2 μm is lower than the linewidth corresponding to 13.2 MHz at 1.55-μm pump wavelength.[10,29] The Brillouin linewidth of the GAST fiber is estimated to be less than 25 MHz according to the known As_2S_3 fiber with the widest linewidth, the Brillouin effects with silica and other chalcogenide fibers are compared with each other, and the value is further calculated here. The A_{eff} of the small-core GAST fiber is less than 15.34 μm^2 with 4-μm-core diameter. The small core structure concentrates the optical field in the core and improves the optic–acoustic coupling efficiency. The n_{eff} of the GAST fiber at 2-μm wavelength is 3.19, which is much larger than the counterparts of other silica and chalcogenide fibers, so the calculated NA of the fiber is much larger than that of chalcogenide fiber. Moreover, V of the GAST fiber is also similar to that of chalcogenide fiber, indicating that the number of their transmission modes is an approximate value. The g_B of the GAST fiber is 3.81×10^{-9} m/W and the SBS efficiency g_B/A_{eff} is as high as 248 m^{-1}. The g_B/A_{eff} is larger than those of the above-mentioned fibers as shown in Table 2.

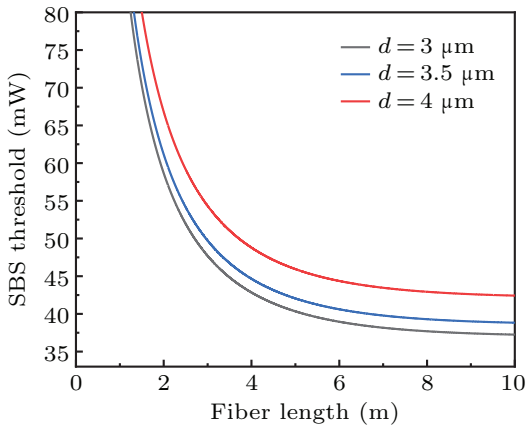


Fig. 8. Curves of Brillouin threshold power *versus* length of GAST fiber with different core diameters.

Table 2. Comparison of parameters related to SBS characteristics of step-index fibers with different glass matrices.

Parameter	SMF-28	As_2S_3	As_2Se_3	TZN	GAST
Wavelength, λ (μm)	2	2	1.55	2	2
Core diameter (μm)	8.2	6.1	6	4	4
Effective index, n_{eff}	1.44	2.443	2.81	1.944	3.19
NA	0.14	0.26	0.18	0.7	0.37
V-number	1.8	2.5	2.2	4.4	2.3
Fiber loss ($dB{\cdot}m^{-1}$)	0.022	0.2	0.84	0.5	3
Length (m)	500	2	5	2	2
Effective length, L_{eff} (m)	180	1.91	3.2	1.79	1.27
Effective area, A_{eff} (μm^2)	101	26	39	10	15.34
Brillouin frequency shift, f_B (GHz)	8.4	6.21	7.95	6.17	7.02
Brillouin linewidth, Δf_B (MHz)	15	25	13.2	15	25[b]
Calculated Brillouin gain coefficient, g_B (10^{-9} $m{\cdot}W^{-1}$)	0.025	1.17	6.08	0.13	3.81
Calculated SBS efficiency, g_B/A_{eff} ($m^{-1}{\cdot}W^{-1}$)	0.25	45	156	13	248
Calculated SBS threshold, P_{th} (mW)	13000[a]	90[a]	85	420[a]	66
Reference	[10]	[10]	[9]	[10,31]	this work

[a]Calculated from 10-m-long fiber segment in Ref. [10]. [b]Estimated from maximum linewidth of fiber in table.

Table 2 demonstrates that the estimated Brillouin threshold power for the GAST fiber of 2 m is roughly 66 mW, which is much lower than that of As_2S_3 fiber. This is because the large nonlinear characteristics of the GAST fiber compensate for the deficiency of the fiber loss compared with other fibers, thereby improving the SBS efficiency. Ultimately, better Brillouin effect can be achieved by further reducing the fiber loss. Finally, the BGS peak of GAST fiber reaches a relatively high value of 373×10^{-11} m/W, indicating that the increase of core refractive index is more conducive to significantly enhancing the BGS value.

5. Conclusions

In this work, we prepared GAST glass with high refractive index at 2 μm, simulated the characteristics of the SBS with varying core diameters on the basis of the step-index GAST fiber, and further analyzed the coupling mechanism of higher-order acoustic modes in the acoustic field and optical field for the first time. The simulation results show that the optic–acoustic coupling efficiency is close to 1 in the fundamental acoustic mode of step-index GAST fiber. In the single-mode optical transmission, the optic–acoustic coupling efficiency and BFS difference of the higher-order mode with a smaller core diameter are high and significant. The Brillouin threshold power of GAST fiber is calculated to be 66 mW when the fiber loss is 3 dB/m. The Brillouin gain coefficient is 3.81×10^{-9} m/W and the calculated SBS efficiency is as high as 248 $m^{-1}{\cdot}W^{-1}$, which are substantially higher than those of the reported chalcogenide fibers. The GAST glass with good transparency and high refractive index at 2-μm wavelength offers great possibilities for selecting gain medium for Brillouin fiber laser. Simultaneously, the SBS properties corresponding to various higher-order acoustic fields in GAST fiber offer potential applications in multi parameter sensing.

Acknowledgements

Project supported by the National Natural Science Foundation of China (Grant Nos. 61875094 and 62090064), the China Postdoctoral Science Foundation (Grant No. 2018M642386), and the K. C. Wong Magna Fund in Ningbo University.

References

[1] Leng J Y, Chen S P, Wu W M, Hou J and Xu X J 2011 *Opt. Commun.* **284** 2997
[2] Mihelic F, Bacquet D, Zemmouri J and Szriftgiser P 2010 *Opt. Lett.* **35** 432
[3] Rossi L, Marini D, Bastianini F and Bolognini G 2019 *Opt. Express* **27** 29447
[4] Tanemura T, Takushima Y and Kikuchi K 2002 *Opt. Lett.* **27** 1552
[5] Huang S H, Zhu T, Yin G L, Lan T Y, Huang L G, Li F H, Bai Y Z, Qu D R, Huang X B and Qiu F 2017 *Opt. Lett.* **42** 5286
[6] Luo Y F, Tang Y L, Yang J L, Wang Y, Wang S W, Tao K Y, Zhan L and Xu J Q 2014 *Opt. Lett.* **39** 2626
[7] Wang X, Zhou P, Wang X L, Xiao H and Si L 2014 *IEEE Photon. J.* **6** 1
[8] Kobyakov A, Kumar S, Chowdhury D Q, Ruffin A B, Sauer M, Bickham S R and Mishra R 2005 *Opt. Express* **13** 5338
[9] Abedin K S 2005 *Opt. Express* **13** 10266
[10] Deroh M, Beugnot J C, Hammani K, Finot C, Fatome J, Smektala F, Maillotte H, Sylvestre T and Kibler B 2020 *J. Opt. Soc. Am. B* **37** 3792
[11] Florea C, Bashkansky M, Dutton Z, Sanghera J, Pureza P and Aggarwal I 2006 *Opt. Express* **14** 12063
[12] Tow K H, Leguillon Y, Fresnel S, Besnard P, Brilland L, Mechin D, Toupin P and Troles J 2013 *IEEE Photon. Technol. Lett.* **25** 238
[13] Wang Y Y, Xu L L, Jiang L, Dai S X, Yang P L and Yi L L 2021 *Opt. Commun.* **484** 126678
[14] Hu K, Kabakova I V, Büttner T F S, Lefrancois S, Hudson D D, He S and Eggleton B J 2014 *Opt. Lett.* **39** 4651
[15] Liu J, Jiao K, Xu T S, Liang X L, Zhong M H, Wang X G, Zhao Z M, Si N, Tian Y M, Wang R P, Shen X and Wang X S 2020 *Spectrochim. Acta A Mol. Biomol. Spectrosc.* **229** 117885
[16] Peng X F, Jiang L, Li G T, Yuan Y, Wang Y Y, Dai S X, Zhang N, Su J X, Yang P L and Zhang P Q 2019 *J. Non. Cryst. Solids* **525** 119690

[17] Jiang C, Wang X S, Zhu M M, Xu H J, Nie Q H, Dai S X, Tao G M, Shen X, Cheng C, Zhu Q D, Liao F X, Zhang P Q, Zhang P Q, Liu Z J and Zhang X H 2016 *Opt. Eng.* **55** 56114
[18] Agrawal G P 2000 *Nonlinear Science at the Dawn of the* 21*st Century* (Berlin: Springer) p. 195
[19] Boyd R W 2020 *Nonlinear optics* (London: Academic Press) p. 419
[20] Silva R E, Franco M A R, Bartelt H and Pohl A A P 2013 *Workshop on Specialty Optical Fibers and their Applications*, August 28–30, 2013, Sigtuna, Sweden, p. F2.20
[21] Cheng T L, Liao M S, Gao W Q, Duan Z C, Suzuki T and Ohishi Y 2012 *Opt. Express* **20** 28846
[22] Wang X, Zhou P, Wang X L, Xiao H and Si L 2013 *Opt. Express* **21** 32386
[23] Chen X, Xia L, Li W and Li C 2017 *Chin Opt Lett* **15** 42901
[24] Cherif R, Zghal M and Tartara L 2012 *Opt. Commun.* **285** 341
[25] Zhong M H, Liang X L, Jiao K, Wang X G, Si N, Xu T S, Xiao J, Liu J, Yang P L, Zhao Z M, Wang X S, Wang R P, Zhou Y X, Zhang P Q, Liu Y X and Nie Q H 2022 *J. Light. Technol.* **38** 4533
[26] Baili A, Cherif R, Salem A B, Kumar A, Sinha R and Zghal M 2015 *Photonic Fiber and Crystal Devices: Advances in Materials and Innovations in Device Applications IX*, August 26, 2015, California, USA, p. 136
[27] Li L J, Lai Y Z, Cao M Y, Yuan X M, Xu Z, Guan J P, Jing S and Jing L 2013 *Acta Phys. Sin.* **62** 140201 (in Chinese)
[28] Cao M, Huang L, Tang M, Mi Y A and Ren G B 2020 *Opt. Lett.* **45** 1427
[29] Shiryaev V, Churbanov M, Dianov E, Plotnichenko V, Adam J and Lucas J 2005 *J. Optoelectron. Adv. M.* **7** 1773
[30] Strutynski C, Picot-Clémente J, Lemiere A, Froidevaux P, Désévédavy F, Gadret G, Jules J C, Kibler B and Smektala F 2016 *J. Opt. Soc. Am. B* **33** D12
[31] Cheng T L, Cherif R, Liao M S, Gao W Q, Duan Z C, Zghal M, Suzuki T and Ohishi Y 2012 *Appl. Phys. Express* **5** 102501